Article

Inferring Snow Water Equivalent for a Snow-Covered Ground Reflector Using GPS Multipath Signals

Mark D. Jacobson

Montana State University Billings, 1500 University Drive, Billings, MT 59101, USA;
E-Mail: mjacobson@msubillings.edu; Tel.: +1-406-657-2203; Fax: +1-406-657-2829

Abstract: A nonlinear least squares fitting algorithm is used to estimate both snow depth and snow density for a snow-layer above a flat ground reflector. The product of these two quantities, snow depth and density, provides an estimate of the snow water equivalent. The input to this algorithm is a simple ray model that includes a speculary reflected signal along with a direct signal. These signals are transmitted from the global positioning system satellites at 1.57542 GHz with right-hand circularly polarization. The elevation angles of interest at the GPS receiving antenna are between $5°$ and $30°$. The results from this nonlinear algorithm show potential for inferring snow water equivalent using GPS multipath signals.

Keywords: global positioning system (GPS); multipath; specular reflection; snow depth; snow density; snow water equivalent

1. Introduction

Snow depth and snow density measurements are important for seasonal snow-covered regions. The product of snow depth and density is called the snow water equivalent (SWE). This quantity, SWE, is the single most important parameter for hydrological studies because it represents the amount of water potentially available for runoff. A measurement of water stored in the snowpack is necessary for fresh water budget estimation. These estimations are used for the management of water supply and flood control systems. In the United States, the Department of Agriculture, Natural Resources Conservation Service, National Water and Climate Center operates and manages the Snowpack Telemetry (SNOTEL) system [1–3]. For approximately 30 years, this system has provided critical high elevation climate information from the major water yield areas of the mountainous West. Two of SNOTEL's

measurements are snow depth and SWE. Snow depth is measured by a sonic sensor, while SWE is measured by a snow pillow device and a pressure transducer. Currently, this network operates 730 remote sites in the Western United Sates including Alaska. In order to increase the spatial coverage of snow properties in these regions, remote sensing instruments on ground-based, airborne and space platforms are being used to supplement the SNOTEL sites [4].

Recently, it has been reported that reflected GPS signals can provide useful information about the land-surface composition such as snow depth, lake ice thickness, soil moisture, ground electrical characteristics, or sea ice conditions [4–22]. The possibility of estimating dry snow density with the GPS L1 frequency was first mentioned by Jacobson [5]. Larson *et al.* [4] are also attempting to estimate dry snow density with GPS multipath signals. This paper outlines a technique for estimating both dry snow density and snow depth (and therefore SWE) for a snow-covered ground reflector. *In situ* snow depth measurements are compared with the inferred technique results. Unfortunately, no snow density measurements were taken during the experiment. Therefore, comparisons between with *in situ* snow density measurements and the inferred method results are not possible. Estimating SWE for a snow layer above frozen soil is also explored.

2. SWE Estimation

2.1. With a Ground Reflector

The relative received power (*P*) at a GPS receiver for a snow-covered conducting plate model, as described by Jacobson [5], is used as the fitting function in a quasi—Newton algorithm (QNA) [23]. This algorithm is used to estimate two nonlinear parameters, snow depth and snow density, in a least-squares sense. The model for calculating *P* includes a vertically-mounted hemispherical directional antenna with no sidelobes, a smooth snow layer of infinite extent, a perfectly conducting flat surface (ground reflector) of infinite extent (the experiment uses a very small ground reflector), and uniform plane waves with a monochromatic frequency. Figure 1 illustrates the total field received by the GPS antenna. The total field is the sum of the direct and specularly-reflected signals. Reflected signals arrive at GPS receivers either coherently or incoherently depending on the roughness of the surface. Coherently reflected signals are caused by smooth surfaces and are called specularly-reflected signals. Most of the reflected signal occurs within the first Fresnel zone about the specular point. In contrast, incoherent reflected signals are caused by rough surfaces and are called diffusely scattered signals.

A vertically-mounted antenna, with the maximum of the main lobe in the horizontal direction (elevation angle of 0 °), is chosen to provide equal antenna gain from the directions of the direct and reflected GPS signals. The active Trimble antenna (50.5 mm × 42.0 mm × 13.8 mm) consists of a microstrip patch antenna, a preamplifier, a radome and a ground plane. The calculation of the total field is simplified with equal antenna gains for the direct and reflected signals. With a vertically-mounted antenna, the received GPS signal strength increases with decreasing elevation angle because the actual antenna gain pattern increases with decreasing elevation angle. In fact, the measured half-power beamwidth of the antenna is approximately 120 °. In addition, the antenna gain decreases by approximately 10 dB at 90 ° away from the maximum of the main lobe. These low elevation angles provide the greatest effect on the reflected signals because the electrical path length of the GPS signal

in the snow increases as the elevation angle decreases. As a practical matter, snow or ice accumulation on top of a vertically-mounted antenna will be less than a horizontally-mounted antenna (maximum of the main lobe in the zenith direction) because there is less antenna surface area exposed to the zenith direction. The disadvantage of a vertically-mounted antenna is that ground-based operational GPS antennas are always pointed to zenith (*i.e.*, antenna is horizontally-mounted). Zenith-pointing antennas maximize the number of viewable GPS satellites and also minimize multipath effects. This paper however uses a vertically-mounted antenna for the reasons given above. Therefore, the relative received power at the right-hand circularly polarized antenna [24] is

$$P = \left| 1 + \frac{(r_h - r_v)}{2} \exp(i\phi) \right|^2 \tag{1}$$

where r_h is the field reflection at horizontal polarization; r_v is the field reflection at vertical polarization; $\phi = \dfrac{4\pi(h-t)\sin\theta}{\lambda_0}$ is the phase shift difference in physical path length between the direct and reflected paths [25]; $i = \sqrt{-1}$ is the definition of i; h is the height of antenna above conducting surface (m); t is the snow layer thickness (m); θ is the elevation angle (degrees); $c = 2.997925 \times 10^8$ m/s is the speed of light in a vacuum; $f = 1.57542$ GHz is the GPS L1 frequency; and $\lambda_0 = c/f = 0.1902937$ m is the GPS L1 free-space wavelength.

Figure 1. Geometry of the total GPS L1 signal at the receiving antenna with a height h above a perfect ground reflector. Snow layer has a thickness of t. The elevation angle is given by θ.
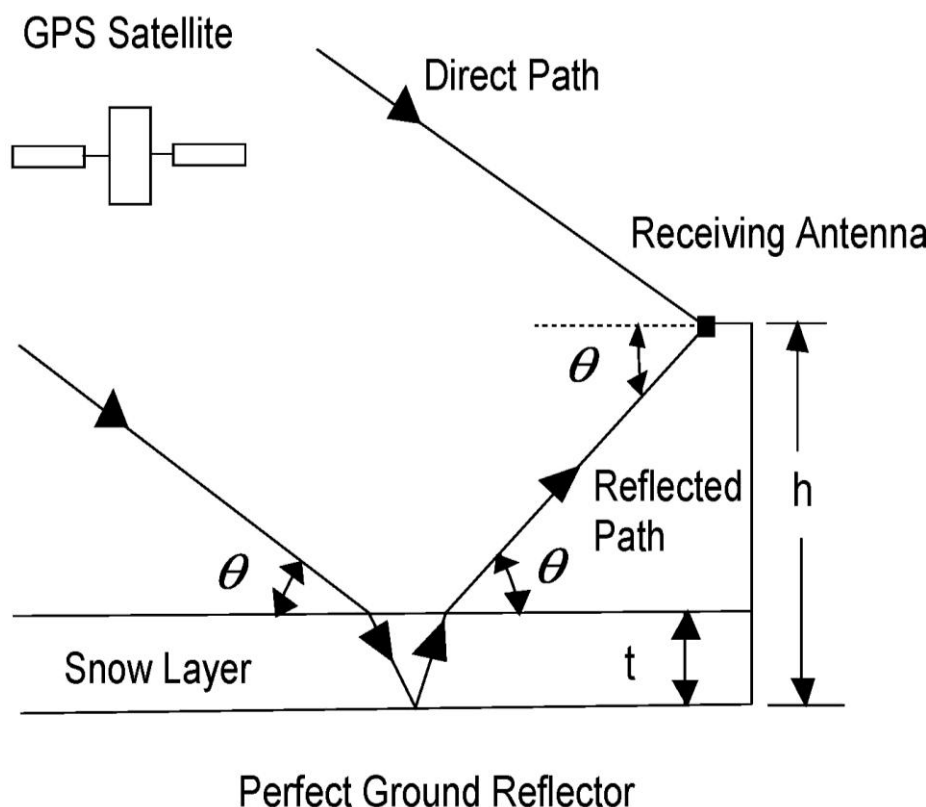
With this model, we compute r_h and r_v by using a ray diagram [5]

$$r_x = \frac{iZ_x \tan\psi - 1}{iZ_x \tan\psi + 1} \text{ for } x = h \text{ or } v \tag{2}$$

$$\text{where } Z_h = \frac{\sin\theta}{\sqrt{\varepsilon - \cos^2\theta}} \tag{3}$$

$$Z_v = \frac{\sqrt{\varepsilon - \cos^2\theta}}{\varepsilon \sin\theta} \tag{4}$$

$$\psi = \frac{2\pi}{\lambda_0} t \sqrt{\varepsilon - \cos^2\theta} \tag{5}$$

where ε is the relative complex permittivity of dry snow. The relative complex permittivity value of dry snow is computed from Tiuri's microwave dry snow model [26]

$$\varepsilon = \varepsilon_{snow} = \varepsilon_s' - i\varepsilon_s'' \tag{6}$$

$$\text{where } \varepsilon_s' = 1 + 2\rho_d \tag{7}$$

$$\varepsilon_s'' = \varepsilon_s' \times 1.59 \times 10^6 \times \frac{0.52\rho_d + 0.62(\rho_d)^2}{1 + 1.7\rho_d + 0.7(\rho_d)^2} \times \left(f^{-1} + 1.23 \times 10^{-14}\sqrt{f}\right) e^{0.036T} \tag{8}$$

where ρ_d is the relative density of dry snow in g cm^{-3}; and T is the temperature of snow in degrees C.

The measured data from a snow-covered reflector [5] are fitted with the above fitting function P in a QNA. Figure 2 is a photograph of the snow-covered ground reflector used in this experiment. The aluminum ground reflector has dimensions of approximately 5 m × 5 m. The ground reflector consists of sixteen 1.22 m × 1.22 m plywood sections covered by heavy duty aluminum foil. This ground reflector was screwed into twenty-seven 10.2 cm × 10.2 cm × 1.83 m plastic fence posts. This provided a reasonably flat surface for the ground reflector. The antenna was mounted on a tripod at the middle of one edge of the ground reflector. Therefore the antenna's beam illuminated the entire ground reflector. The site was located in terrain that minimized blockage and shadowing. Signal power levels in both measurements and simulation results have been normalized. Power levels were directly recorded in decibels (dB) from the GPS receiver every 0.5 seconds to a laptop computer.

The site was located 13 km west of Billings, MT. The measurements were performed on March 31, 2007 with partly cloudy skies between 14:44 and 15:52 GPS time for satellite PRN 4. The wind-blown snow layer was from a two-day storm that occurred on March 28 and 30, 2007. The snow depth was approximately 7.6 cm ± 2.5 cm. The snow depth on the ground reflector was measured with a ruler approximately every 2.5 m with one corner as the origin, see Table 1. The snow temperature increased from −3.3 °C to 0.0 °C during this time. Therefore, an average snow temperature of −1.7 °C was chosen for the model. For this paper, the elevation angles were restricted to be between 5° and 30° in order to maximize the multipath effects from the snow layer. This occurs because the electrical path length of the GPS signal through the snow increases as the elevation angle decreases. This elevation range is similar to that chosen by Larson *et al.* [4]. This elevation angle range yields 8,168 data points.

The antenna was mounted on a tripod above the air-snow interface at a height of approximately 38.3 cm (for $t = 6.8$ cm and $h = 45.1$ cm). Since this is just several wavelengths away from the ground

reflector (*i.e.*, in the near field of the receiving antenna), the area that contributes into reflection might be somewhat larger. Although the geometric optics approximation may be marginal for this situation, we use it as a first-order estimate. Further studies will assess the accuracy of this method. With this in mind, we use the far field (Fraunhofer diffraction), first Fresnel zone dimensions for estimating the effectiveness of the ground reflector dimensions. With an antenna height of 38.3 cm and an elevation angle of 15°, the first Fresnel zone [26] is calculated to have a major axis length of approximately 5 m and a minor axis length of approximately 1.5 m. Therefore, the first Fresnel zone lies entirely on the snow-covered reflector for elevations angles $\geq 15°$. On the other hand, at an elevation angle of 5° (lowest elevation angle in the measurements), the first Fresnel zone is calculated to have a major axis length of approximately 34 m and a minor axis length of approximately 3 m. Therefore, the first Fresnel zone lies on both the snow-covered reflector and the snow-covered frozen ground for elevations angles $< 15°$. This indicates that the ground reflector is not large enough for the smaller elevation angles. The measurements indicate that this is not a severe problem. The reflector size design was chosen because of money, time and labor constraints.

Figure 2. Snow-covered ground reflector. The antenna is mounted vertically on the tripod with $h = 45.1$ cm.

Table 1. Nine snow depth (*t*) measurements taken from the base of the ground reflector using a ruler. One corner location is assigned the origin value of (0, 0) in (m). The measured snow depth range is 7.6 cm ± 2.5 cm.

x, y (m)	(0, 0)	(0, 2.5)	(0, 5)	(2.5, 0)	(2.5,2.5)	(2.5, 5)	(5, 0)	(5, 2.5)	(5, 5)
t (cm)	7.0	7.3	5.1	8.5	9.4	10.1	6.4	5.7	9.1

In order to utilize a QNA efficiently in finding estimates of snow depth and density, we approximate the relative complex permittivity value of dry snow as [26]

$$\varepsilon_{snow} = \varepsilon_s^{'} - i\varepsilon_s^{''} \approx \varepsilon_s^{'} = 1 + 2\rho_d \tag{9}$$

because

$$\varepsilon_s^{''} \ll \varepsilon_s^{'} \tag{10}$$

The snow depth and the approximate dry snow permittivity value are used as the two inputs to the fitting function *P* in a QNA. Notice the simple linear relationship in (9) between snow permittivity and snow density. The following snow depth and permittivity values are chosen to bracket the measured and typical values of this experiment. The following 9 snow depth values (*t*) are used as QNA inputs: 2.54, 5.1, 7.6, 10.1, 20.0, 30.0, 40.0, 50.0, and 100.0 cm. In addition, the following 5 snow permittivity values (ε_{snow}) are used as QNA inputs: 1.3, 1.38, 1.48, 1.68, and 1.80. These values produce 45 different paired combinations of snow depth and snow permittivity.

Each pair of snow depth and permittivity value is used as an input to a QNA. The output of a QNA produces a snow depth, a permittivity value and a standard error (SE) by performing a nonlinear least squares fit between theory and measurement. The process for calculating the SE for each output pair of QNA is given by the following expression

$$SE(t, \varepsilon_{snow}) = min\left\{\sqrt{\frac{1}{n-2}\sum_{i=1}^{i=n}[y(\theta_i) - P(\theta_i, t, \varepsilon_{snow})]^2}\right\} \tag{11}$$

where *y* is the measured power value in dB, *P* is the fitting function in dB, *t* is the snow depth in m, ε_{snow} is the snow permittivity value, θ is the elevation angle in degrees, *n* is the number of data points (8168), and *min* is the abbreviation for minimize.

This procedure is performed for all 45 paired combinations. The best estimate of snow depth and permittivity (density) is determined by which QNA output produces the smallest SE. Table 2 is a summary of the paired input combinations and corresponding output results. A snow depth of 6.8 cm and a snow density of 0.30 g cm^{-3} produces the smallest SE of 1.146 dB; the resulting SWE = 2.04 g cm^{-2} = 20.4 kg m^{-2}. This output pair value occurs about 30% of the time (the most frequent output pair) and is shown in bold in Table 2. This inferred snow depth of 6.8 cm is within the measured depth range of 7.6 cm ± 2.5 cm. Furthermore, the inferred snow density of 0.30 g cm^{-3} is typical for this region at this time of year (0.20–0.40 g cm^{-3}) [4,27,28]; unfortunately, no snow density measurements were taken. Figure 3 shows two-dimensional contour plots of the QNA output values produced by the 45 input pairs.

Table 2. Summary of the output values of snow depth (*t*), snow permittivity (ε_{snow}), snow density (ρ_d) and standard error (SE) produced by 45 paired input combinations of snow depth and permittivity using a quasi-Newton algorithm (QNA). The bold entries indicate the smallest SE result of 1.146, which corresponds to output values of snow depth and snow density of 6.8 cm and 0.3 g cm^{-3}, respectively.

INPUT		OUTPUT			
t (cm)	ε_{snow}	*t* (cm)	ε_{snow}	ρ_d (g cm^{-3})	SE (dB)
2.54	1.3	3.53	1.3	0.15	1.378
2.54	1.38	3.56	1.4	0.13	1.277
2.54	1.48	3.53	1.3	0.15	1.378
2.54	1.68	3.53	1.3	0.15	1.378
2.54	1.8	3.53	1.3	0.15	1.378
5.1	1.3	3.53	1.3	0.15	1.378
5.1	1.38	3.53	1.3	0.15	1.378
5.1	1.48	3.8	1.27	0.083	1.161
5.1	**1.68**	**6.8**	**1.6**	**0.3**	**1.146**
5.1	**1.8**	**6.8**	**1.6**	**0.3**	**1.146**
7.6	**1.3**	**6.8**	**1.6**	**0.3**	**1.146**
7.6	**1.38**	**6.8**	**1.6**	**0.3**	**1.146**
7.6	**1.48**	**6.8**	**1.6**	**0.3**	**1.146**
7.6	**1.68**	**6.8**	**1.6**	**0.3**	**1.146**
7.6	**1.8**	**6.8**	**1.6**	**0.3**	**1.146**
10.1	**1.3**	**6.8**	**1.6**	**0.3**	**1.146**
10.1	**1.38**	**6.8**	**1.6**	**0.3**	**1.146**
10.1	1.48	3.4	1.3	0.13	1.334
10.1	1.68	3.5	1.26	0.13	1.28
10.1	1.8	3.4	1.27	0.13	1.334
20.0	1.3	0	1.15	0.08	2.752
20.0	1.38	0	1.42	0.21	3.051
20.0	1.48	3.4	1.28	0.14	1.349
20.0	1.68	0.04	1.63	0.11	1.261
20.0	1.8	3.8	1.28	0.14	1.351
30.0	1.3	2.4	1.15	0.074	2.411
30.0	1.38	11.0	1.8	0.4	2.105
30.0	1.48	3.4	1.28	0.14	1.349
30.0	**1.68**	**6.8**	**1.6**	**0.3**	**1.146**
30.0	**1.8**	**6.8**	**1.6**	**0.3**	**1.146**
40.0	1.3	27.6	1.39	0.2	3.426
40.0	1.38	26.8	1.72	0.36	3.195
40.0	1.48	10.5	1.8	0.4	2.105
40.0	1.68	10.5	1.8	0.4	2.105
40.0	**1.8**	**6.8**	**1.6**	**0.3**	**1.146**
50.0	1.3	50.4	1.3	0.15	2.845
50.0	1.38	3.53	1.3	0.15	1.378

Table 2. *Cont.*

INPUT		OUTPUT			
t (cm)	ε_{snow}	*t* (cm)	ε_{snow}	ρ_d (g cm^{-3})	SE (dB)
50.0	1.48	52.9	1.5	0.25	2.8
50.0	1.68	11.0	1.8	0.4	2.105
50.0	**1.8**	**6.8**	**1.6**	**0.3**	**1.146**
100.0	1.3	86.5	1.3	0.15	1.972
100.0	1.38	3.73	1.27	0.14	1.307
100.0	1.48	3.53	1.3	0.15	1.378
100.0	1.68	88.2	1.87	0.44	2.761
100.0	1.8	89.4	1.8	0.4	2.535

Figure 3. (a) Two-dimensional contour plot of snow depth (*t*) and snow density (ρ_d) with contour values of standard error (SE) of the QNA output values produced by the 45 input pair combinations of snow depth and permittivity (ε_{snow}) in Table 2 using a quasi-Newton algorithm (QNA). The purple regions show the smallest SE. **(b)** Expanded view of **(a)** for output snow depths between 0 and 10 cm.

(a)

Figure 3. *Cont.*

(b)
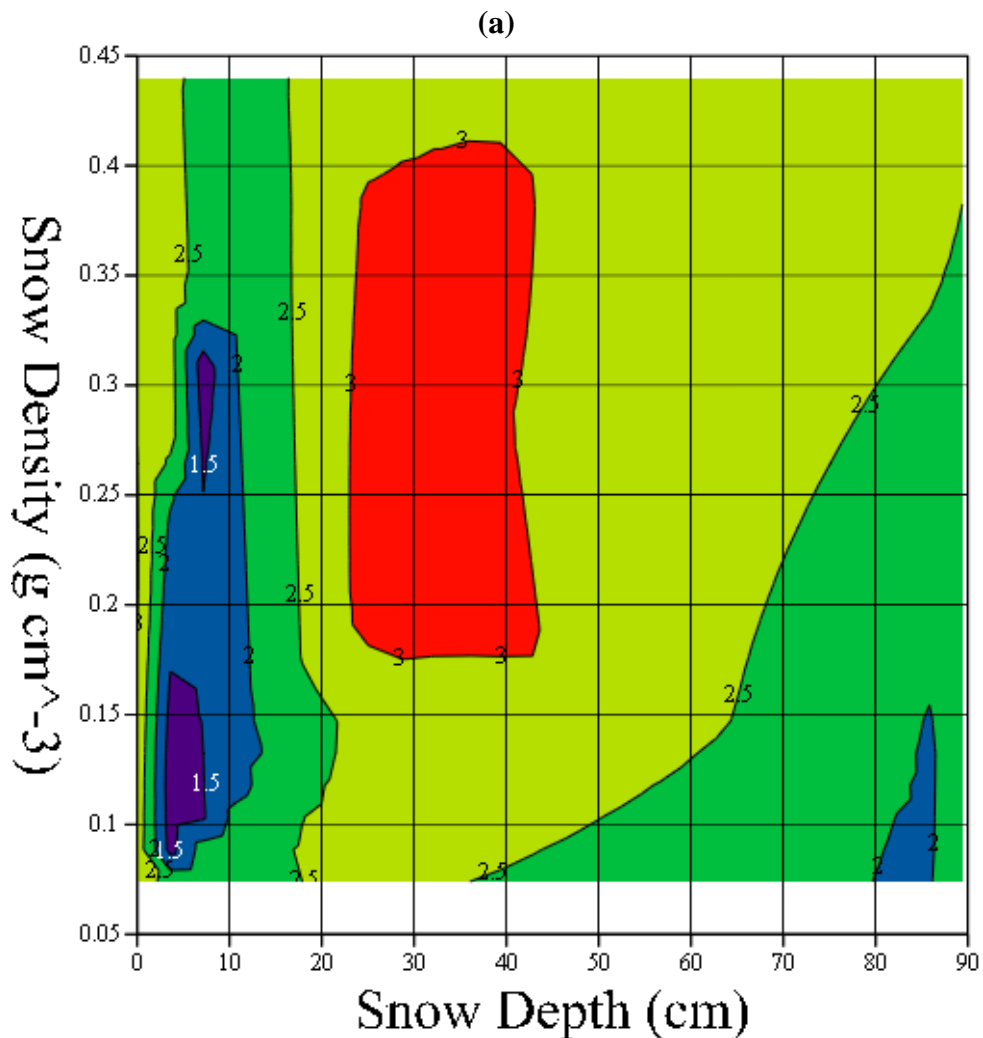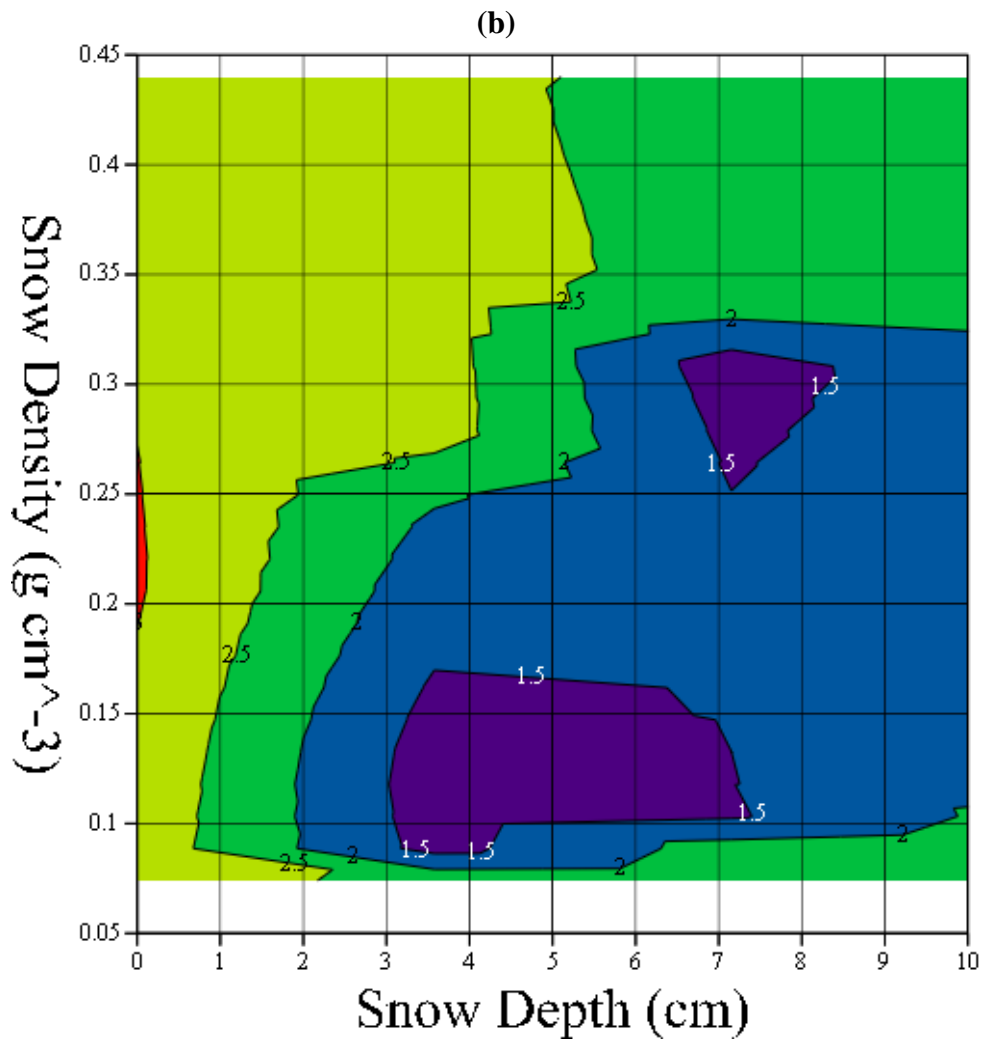
Figure 4 shows the measurement and theoretical results for 6.8- and 7.6-cm-thick snow layers. The 7.6-cm-thick snow layer was used as the best fit to the data in [5], and is shown here for comparison purposes. The snow densities for the 6.8- and 7.6-cm-thick snow layers are 0.30 and 0.24 g cm^{-3}, respectively. The corresponding relative permittivity values [26] for the 6.8- and 7.6-cm-thick snow layers are $\varepsilon_{snow} = 1.60 - i3.58 \times 10^{-4}$ and $\varepsilon_{snow} = 1.48 - i2.76 \times 10^{-4}$, respectively. The results shown here provide evidence that estimates of snow depth and density (and therefore SWE) may be possible using GPS multipath signals. However, it should be noted that this technique requires several input guess values for snow depth and permittivity (density) to determine which output pair produces the minimum SE.

Figure 4. (Lines) Theoretical and (square) measured elevation plots for a ground reflector covered by 6.8- and 7.6-cm-thick snow layers with $h = 45.1$ cm for the GPS satellite PRN 4. The values $\varepsilon_{\text{snow}} = 1.60 - i3.58 \times 10^{-4}$ and $\varepsilon_{\text{snow}} = 1.48 - i2.76 \times 10^{-4}$ are used in the 6.8- and 7.6-cm-thick snow layer models, respectively. The GPS times from the measurements are 14:44 to 15:52.
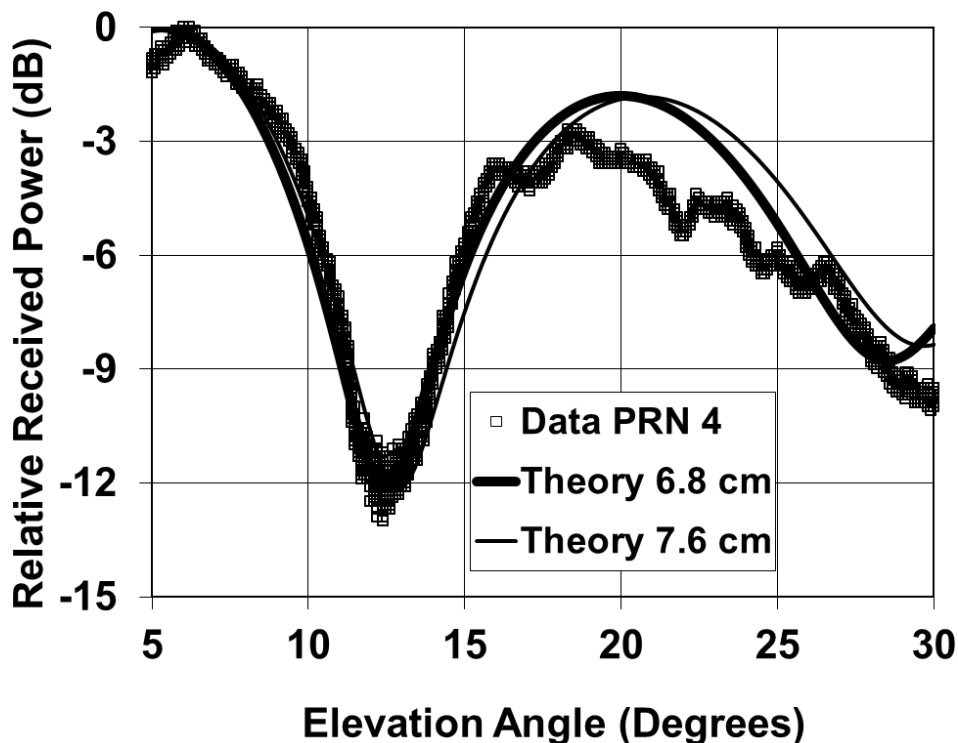
2.2. Without a Ground Reflector

The possibility of using GPS signals to estimate SWE is investigated further by replacing the perfect ground reflector with smooth, flat frozen soil. This situation was considered in experiments [4] where, unlike here, a commonly used horizontally-mounted GPS antenna was employed. The relative received power (*P*) at a GPS antenna for a snow-covered frozen soil model is computed by using the model described in [6]. The total field is the sum of the direct and specularly-reflected signals. The relative received power at the right-hand circularly polarized antenna is given in (1). The dielectric identifier, *j*, has the following values in this model: 1 for the snow layer and 2 for the frozen soil. The field reflection is

$$r_x = \frac{W_{xj} - 1}{W_{xj} + 1} \text{ , for } x = \text{h or v} \tag{12}$$

where

$$W_{xj} = \frac{Z_{x2} + iZ_{xj} \tan \psi_j}{1 + i\dfrac{Z_{x2}}{Z_{xj}} \tan \psi_j} \tag{13}$$

$$Z_{hj} = \frac{\sin\theta}{\sqrt{\varepsilon_j - \cos^2\theta}} \qquad (14)$$

$$Z_{vj} = \frac{\sqrt{\varepsilon_j - \cos^2\theta}}{\varepsilon_j \sin\theta} \qquad (15)$$

$$\psi_j = \frac{2\pi}{\lambda_0} t \sqrt{\varepsilon_j - \cos^2\theta} \qquad (16)$$

where ε_j is the relative complex permittivity of dry snow or frozen soil, and t is the dry snow layer thickness (m).

We model the relative complex permittivity value of the frozen soil with a constant profile for two different frozen soils given in Hallikainen *et al.* [29]. In particular, the two different frozen soil graphs, Fields 1 and 5 at −11 ℃, are extrapolated to the GPS L1 frequency to yield the following approximate relative complex permittivity values: $\varepsilon_2 = \varepsilon_{soil\,1} = 5 - i0.5$ for Field 1 and $\varepsilon_2 = \varepsilon_{soil\,5} = 10 - i2.0$ for Field 5. The frozen soil characteristics of Fields 1 and 5 are shown in Table 3. A more realistic model of the frozen soil [30] should be implemented for future studies. Figure 5 shows the measurement and theoretical results for the perfect reflector and the two frozen soils. The frozen soils reduce the fade depths as compared to the perfect reflector. In addition, the frozen soils increases the elevation angle values at the first fade depth as compared to the perfect reflector. With these results, a QNA technique might prove useful in estimating SWE for snow-covered frozen soil. In order to implement a QNA, an appropriate snow depth guess value could be obtained by the method outlined by Larson *et al.* [4]. The other guess value, snow density, could be found by using a snow density typical of the region and season. Several other snow depth and density (permittivity) pairs could be selected that would bracket this initial input guess pair value. The SE results from the different paired values may provide an estimate of the SWE. Figure 6 shows the power difference results between the snow-covered perfect reflector and the snow-covered frozen soil from Field 5. The results from this difference plot could possibly be used to estimate the permittivity of the frozen soil under the reflector.

Table 3. Frozen soil characteristics of Fields 1 and 5 as given in [29].

	Sand (%)	Silt (%)	Clay (%)	Volumetric Wetness ($cm^3\,cm^{-3}$)	Bulk Density ($g\,cm^{-3}$)
Field 1	51.5	35.1	13.4	0.24	1.54
Field 5	5	47.6	47.4	0.36	1.42

Figure 5. (Lines) Theoretical and (square) measured elevation plots for a 6.8-cm-thick snow layer covering a ground reflector and two types of frozen soil with $h = 45.1$ cm for the GPS satellite PRN 4. The soil characteristics are given in Table 3. The values $\varepsilon_{snow} = 1.60 - i3.58 \times 10^{-4}$, $\varepsilon_{soil1} = 5 - i0.5$ and $\varepsilon_{soil5} = 10 - i2.0$ are used in the model. The GPS times from the measurements are 14:44 to 15:52.
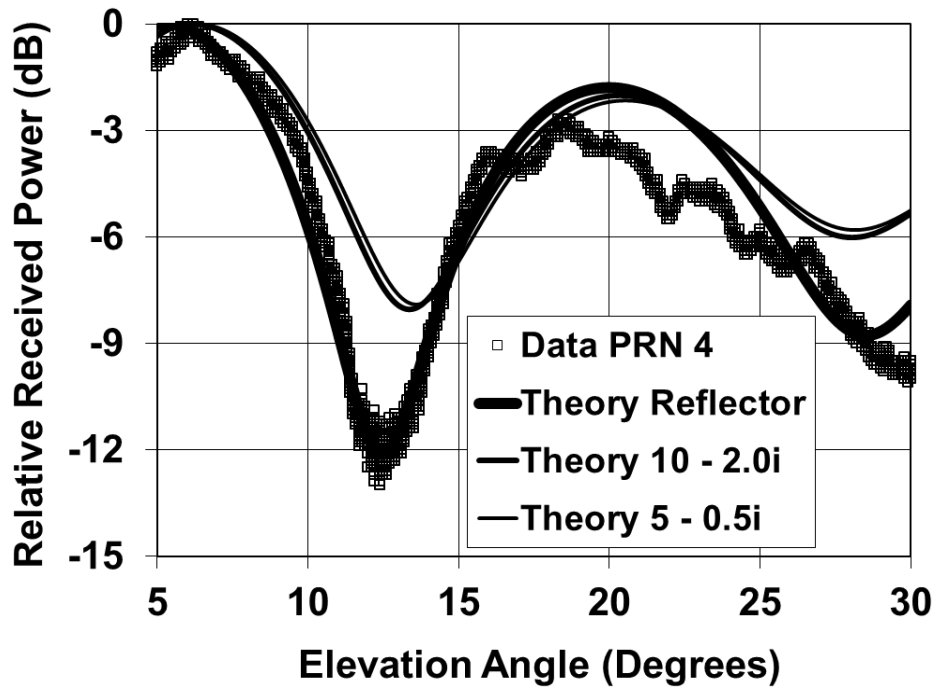
Figure 6. Theoretical elevation plot for the difference between a 6.8-cm-thick snow layer covering a ground reflector and a 6.8-cm-thick snow layer covering frozen soil with a composition of Field 5 with $h = 45.1$ cm. The values $\varepsilon_{snow} = 1.60 - i3.58 \times 10^{-4}$ and $\varepsilon_{soil5} = 10 - i2.0$ are used in the model.
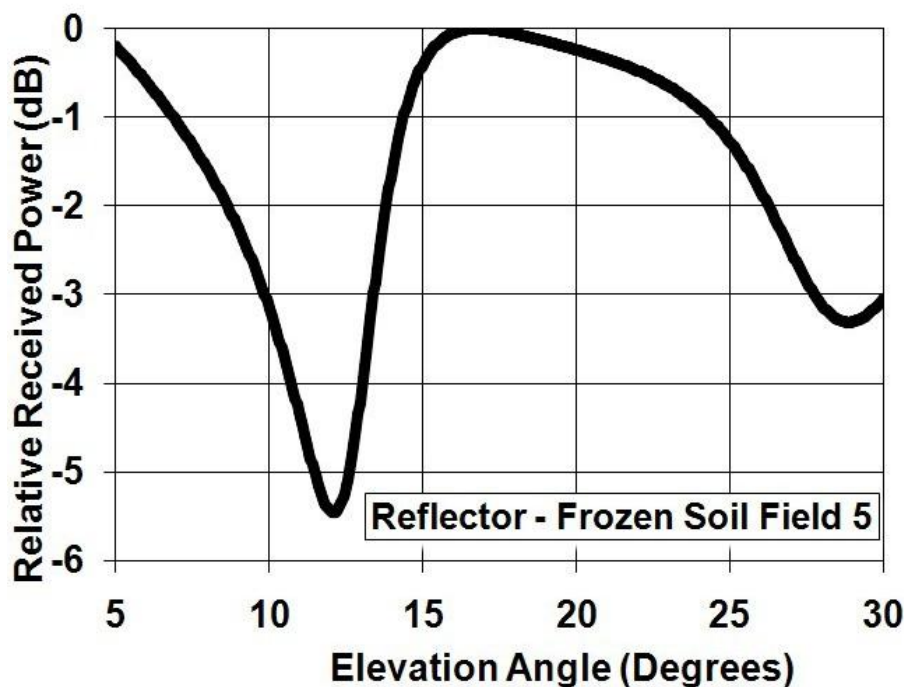
3. Conclusions and Future Research

We investigated a nonlinear least squares fitting technique for inferring both snow depth and snow density for a snow-covered ground reflector using GPS multipath signals. The product of these two parameters provides an estimate of the SWE, which is the most important parameter for hydrological studies because it represents the amount of water potentially available for runoff. A QNA produced a snow depth (6.8 cm) within the *in situ* measurement range, and a snow density (0.30 g cm^{-3}) typical for this region at this time of year. Both theory and measurement show good agreement in the power variations over the elevation angle range between 5° and 30°. This algorithm requires several guess pairs to determine the best least-squares estimate of snow depth and density. Future developments will include making measurements with a larger ground reflector and covering the tripod with microwave absorber. Furthermore, more *in situ* snow depth, snow density, and frozen soil permittivity measurements will be done.

Further studies will compare the performance of other nonlinear algorithms, like the Levenbeg-Marquardt [31] and the conjugate gradient [32] algorithms, to the QNA. In addition, a least squares optimizer needs to be implemented to reduce or to eliminate the need of using input pair values. Continuing research will explore the feasibility of using this technique to infer SWE for a snow layer above frozen soil. This is the typical situation for ground-based, zenith-pointing GPS antennas. This will require further measurements for different snow depths and snow densities in open and mountainous terrains. In addition, a more realistic model of the frozen soil [30] needs to be implemented. Furthermore, the received signals from different GPS satellites at a specific site and over an appropriate time period need to be compared and analyzed. Continuing theoretical developments will incorporate the surface roughness of snow and frozen soil, the antenna beam pattern, the addition of more snow layers, and the configuration of a horizontally-mounted (zenith-pointing) GPS antenna. If SWE can be estimated using this GPS technique without a ground reflector, then it may be more cost-effective than current techniques. Furthermore, it may expand the spatial coverage of SWE measurements that are not currently provided by SNOTEL sites. For example, there are hundreds of geodetic GPS receivers operating in snowy regions in the U.S. [4]. Therefore, some of these GPS receivers could possibly be used to estimate SWE. Lastly, this technique needs to be investigated for GPS receiving antennas housed on an aircraft or satellite. These aircraft or satellite based platforms could provide much more spatial coverage of SWE measurements than the current ground-based SNOTEL sites.

References

1. Schaefer, G.L.; Paetzold, R.F. SNOTEL (SNOwpack TELemetry) and SCAN(Soil Climate Analysis Network). Presented at *Automated Weather Stations for Applications in Agriculture and Water Resources Management: Current Use and Future*, Lincoln, NE, USA, March 2000. Available online: ftp://ftp.wcc.nrcs.usda.gov/downloads/factpub/soils/SNOTEL-SCAN.pdf (accessed on 18 October 2010).
2. Serreze, M.C.; Clark, M.P.; Armstrong, R.L.; McGinnis, D.A.; Pulwarty, R.S. Characteristics of the western United States snowpack from Snowpack Telemetry (SNOTEL) data. *Water Resour. Res.* **1999**, *35*, 2145–2160.
3. Molotch, N.P.; Bales, R.C. SNOTEL representatives in the Rio Grande headwaters on the basis of physiographics and remotely sensed snow cover persistence. *Hydrol. Processes* **2006**, *20*, 723–739.
4. Larson, K.M.; Gutmann, E.; Zavorotny, V.; Braun, J.; Williams, M.; Nievinski, F. Can we measure snow depth with GPS receivers? *Geophys. Res. Lett.* **2009**, *36*, L17502, doi: 10.1029/2009GL039430.
5. Jacobson, M.D. Dielectric-covered ground reflectors in GPS multipath reception—Theory and measurement. *IEEE Geosci. Remote Sens. Lett.* **2008**, *5*, 396–399.
6. Jacobson, M.D. Snow-covered lake ice in GPS multipath reception—Theory and measurement. *Adv. Space Res.* **2010**, *46*, 221–227, doi: 10.1016/j.asr.2009.10.013.
7. Jin, S.; Komjathy, A. GNSS reflectometry and remote sensing: New objectives and results. *Adv. Space Res.* **2010**, *46*, 111–117, doi: 10.1016/j.asr.2010.01.014.
8. Lowe, S.T.; Kroger, P.; Franklin, G.; LaBerecque, J.L.; Lerma, J.; Lough, M.; Marcin, M.R.; Muellerschoen, R.J.; Spitzmesser, D.; Young, L.E. A delay/doppler- mapping receiver system for GPS-reflection remote sensing. *IEEE Trans. Geosci. Remote Sens.* **2003**, *40*, 1150–1163.
9. Grant, M.S.; Acton, S.T.; Katzberg, S.J. Terrain moisture classification using GPS surface-reflected signals. *IEEE Geosci. Remote Sens. Lett.* **2007**, *4*, 41–45.
10. Larson, K.M.; Small, E.E.; Gutmann, E.; Bilich, A.; Braun, J.; Zavorotny, V.U. Use of GPS receivers as a soil moisture network for water cycle studies. *Geophys. Res. Lett.* **2008**, *35*, L24405, doi:10.1029/2008GL036013.
11. Masters, D.; Zavorotny, V.U.; Katzberg, S.J.; Emery, W. GPS signal scattering from land for moisture content determination. In *Proceedings of IEEE 2000 International Geoscience and Remote Sensing Symposium*, Honolulu, HI , USA, 24–28 July 2000, Volume 7, pp. 3090–3092.
12. Kavak, A.; Xu, G.; Vogel, W.J. GPS multipath fade measurements to determine L-band ground reflectivity properties. In *Proceedings of the 20th NASA Propagation Experimenters Meeting*, Fairbanks, AK, USA, 4–6 June 1996, pp. 257–263.
13. Kavak, A.; Vogel, W.J.; Xu, G. Using GPS to measure ground complex permittivity. *Electron. Letters* **1998**, *34*, 254–255.
14. Katzber, S.J.; Torres, O.; Grant, M.S.; Masters, D. Utilizing calibrated GPS reflected signals to estimate soil reflectivity and dielectric constant: Results from SMEX02. *Remote Sens. Environ.* **2006**, *100*, 17–28.

15. Rivas, M.B.; Maslanik, J.A.; Axelrad, P. Bistatic scattering of GPS signals off Arctic sea ice. *IEEE Trans. Geosci. Remote Sens.* **2010**, *48*, 1548–1553, doi:10.1109/TGRS.2009.2029342.

16. Cline, D.; Yueh, S.; Chapman, B.; Stankov, B.; Gasiewski, A.; Masters, D.; Elder, K.; Kelly, R.; Painter, T.H.; Miller, S.; Katzberg, S.; Mahrt, L. NASA Cold Land Processes Experiment (CLPX 2002/03): Airborne remote sensing. *J. Hydrometeorol.* **2009**, *10*, 338–346.

17. Komjathy, A.; Maslanik, J.A.; Zavorotny, V.U.; Axelrad, P.; Katzberg, S.J. Towards GPS surface reflection remote sensing of sea ice conditions. In *Proceedings of Sixth International Conference on Remote Sensing for the Marine and Coastal Environment*, Charleston, SC, USA, 2000; Volume II, pp. 447–456.

18. Komjathy, A.; Maslanik, J.A.; Zavorotny, V.U.; Axelrad, P.; Katzberg, S.J. Sea ice remote sensing using surface reflected GPS signals. In *Proceedings of IEEE 2000 International Geoscience and Remote Sensing Symposium*, Honolulu, HI, USA, 2000, Volume 7, pp. 2855–2857.

19. Gleason, S.; Lowe, S.; Zavorotny, V. Remote sensing using bistatic GNSS reflections. In *GNSS Applications and Methods*; Gleason, S., Gebre-Egziabher, D., Eds.; Artech House: Norwood, MA, USA, 2009.

20. Gleason, S. Towards sea ice remote sensing with space detected GPS signals: Demonstration of technical feasibility and initial consistency check using low resolution sea ice information. *Remote Sensing* **2010**, *2*, 2017–2039, doi:10.3390/rs2082017.

21. Fabra , F.; Cardellach, E.; Nogués, O.; Oliveras, S.; Ribó, S.; Rius, A.; Belmonte-Rivas, M. Sea ice remote sensing with GNSS reflections. *Instrum. Viewpoint* **2009**, *8*, 54.

22. Wiehl, M.; Legresy, R.; Dietrich, R. Potential of reflected GNSS signals for ice sheet remote sensing. *Progress Electromag. Res.* **2003**, *40*, 177–205.

23. Herceg, D.; Krejic, N.; Luzanin, Z. Quasi-Newton's method with correction. *Novi Sad J. Math.* **1996**, *26*, 115–127.

24. Stutzman, W.L. *Polarization in Electromagnetic Systems*; Artech House: Norwood, MA, USA, 1993; pp. 188–200.

25. Beckman, P.; Spizzichino, A. *The Scattering of Electromagnetic Waves from Rough Surfaces*; Artech House: Norwood, MA, USA, 1987; pp. 285–291.

26. Tiuri, M.E.; Sihvola, A.H.; Nyfors, E.G.; Hallikaiken, M.T. The complex dielectric constant of snow at microwave frequencies. *IEEE J. Ocean. Eng.* **1984**, *9*, 377–382.

27. Shi, J.; Dozier, J. Estimation of snow water equivalence using SIR-C/X-SAR, Part I: Inferring snow density and subsurface properties. *IEEE Trans. Geosci. Remote Sens.* **2000**, *38*, 2465–2474.

28. Ulaby, F.T.; Moore, R.K.; Fung, A.K. *Microwave Remote Sensing, Active and Passive*; Artech House: Norwood, MA, USA, 1986; Volume III, pp. 2060–2067.

29. Hallikainen, M.T.; Ulaby, F.T.; Dobson, M.C.; El-Rayes, M.A.; Wu, L.-K. Microwave dielectric behavior of wet soil—Part I: Empirical models and experimental observations. *IEEE Trans. Geosci. Remote Sens.* **1985**, *23*, 25–34.

30. Zavorotny, V.; Larson, K.M.; Braun, J.; Small, E.E.; Gutmann, E.; Bilich, A. A physical model for GPS multipath caused by land reflections: Toward bare soil moisture retrievals. *IEEE J. Sel. Topics Appl. Earth Obs. Remote Sens.* **2010**, *3*, 100–110.

31. Marquardt, D.W. An algorithm for least-squares estimation of nonlinear parameters. *J. Soc. Indust. Appl. Math.* **1963**, *11*, 431–441.

32. Shewchuk, J.R. *An Introduction to the Conjugate Gradient Method without the Agonizing Pain*; Carnegie Mellon University: Pittsburg, PA, USA, August 1994. Available online: http://www.cs.cmu.edu/~quake-papers/painless-conjugate-gradient.pdf (accessed on 18 October 2010).